Article

Widespread small grabens consistent with recent tectonism on Mercury

Benjamin Man [1] ✉, David A. Rothery [1] ✉, Matthew R. Balme [1] ✉, Susan J. Conway [2] ✉ & Jack Wright [3] ✉

Since Mariner 10 first imaged Mercury in 1974, tectonic landforms dominated by shortening structures have been extensively documented. Contractional tectonism on Mercury is thought to have begun early in the planet's history and is theorized to have continued throughout Mercury's geological history, but observational evidence for recent tectonism is limited. Here we report the widespread occurrence of relatively young grabens on Mercury from global mapping of tectonic features using MESSENGER imagery. The identified grabens are about 10 to 150 m deep, tens of kilometres in length and generally less than 1 km wide. We find that the grabens occur as secondary tectonic features on larger compressional tectonic structures, which indicates continued activity of the parent structure. We estimate that they must be ~300 million years old or younger; otherwise, impact gardening would have masked their signature by burial and infilling. The widespread distribution of grabens and their young age supports the continued activity of Mercury's shortening structures into geologically recent times and is consistent with thermochemical evolution models for a slowly cooling planetary interior and prolonged global contraction.

Shortening structures such as wrinkle ridges, lobate scarps and high-relief ridges are abundant and distributed across the surface of Mercury, as confirmed by the Mercury Surface, Space Environment, Geochemistry and Ranging (MESSENGER) mission[1]. Their formation is widely accepted to result from global contraction caused by secular cooling[2,3] but could also be attributed to tidal despinning[4,5], true polar wander[6] or mantle overturn[7] or a combination of some or all of these[8–10]. Regardless of the cause(s), many studies predict that tectonism on Mercury should still be occurring today[9,11–17], yet the only evidence of recent tectonism on Mercury is the identification of 14 lobate scarps that cross-cut Kuiperian (≲280 million years (Ma) old) craters[12] and 39 <10-km-long pristine scarps in the northern hemisphere, observed in Mercury Dual Imaging System (MDIS)[18] narrow-angle camera (NAC) images[16]. Evidence for widespread continued movement on other shortening structures has been lacking.

In this Article, we present the results of a global survey of grabens atop shortening structures (Figs. 1 and 2 and Supplementary Data 1). These shortening structures are a continuum of landforms accepted to be the surface manifestations of thrust faults and folding formed by lithospheric horizontal compression[13,19]. We first mapped all potential shortening structures to produce a global tectonics database with a high level of spatial detail suitable for our study (Fig. 3a and Supplementary Data 2). Next, we filtered and processed all NAC frames with spatial resolution of 150 m pixel^{-1} or better that intersected the structures in our database. We then searched for and catalogued the occurrence of grabens in these NAC frames. We report examples of grabens, their location and global distribution and discuss the distribution of the parent shortening structures on which they are found. We quantify the depths of grabens using shadow measurements[20,21] along with displacement-length scaling and infer their age on the basis of

[1]The Open University, Milton Keynes, UK. [2]Nantes Université, Université d'Angers, Le Mans Université, Laboratoire de Planétologie et Géosciences, Nantes, France. [3]European Space Agency (ESA), European Space Astronomy Centre (ESAC), Villanueva de la Cañada, Madrid, Spain. ✉e-mail: ben.man@open.ac.uk; david.rothery@open.ac.uk; matt.balme@open.ac.uk; susan.conway@univ-nantes.fr; jack.wright@esa.int
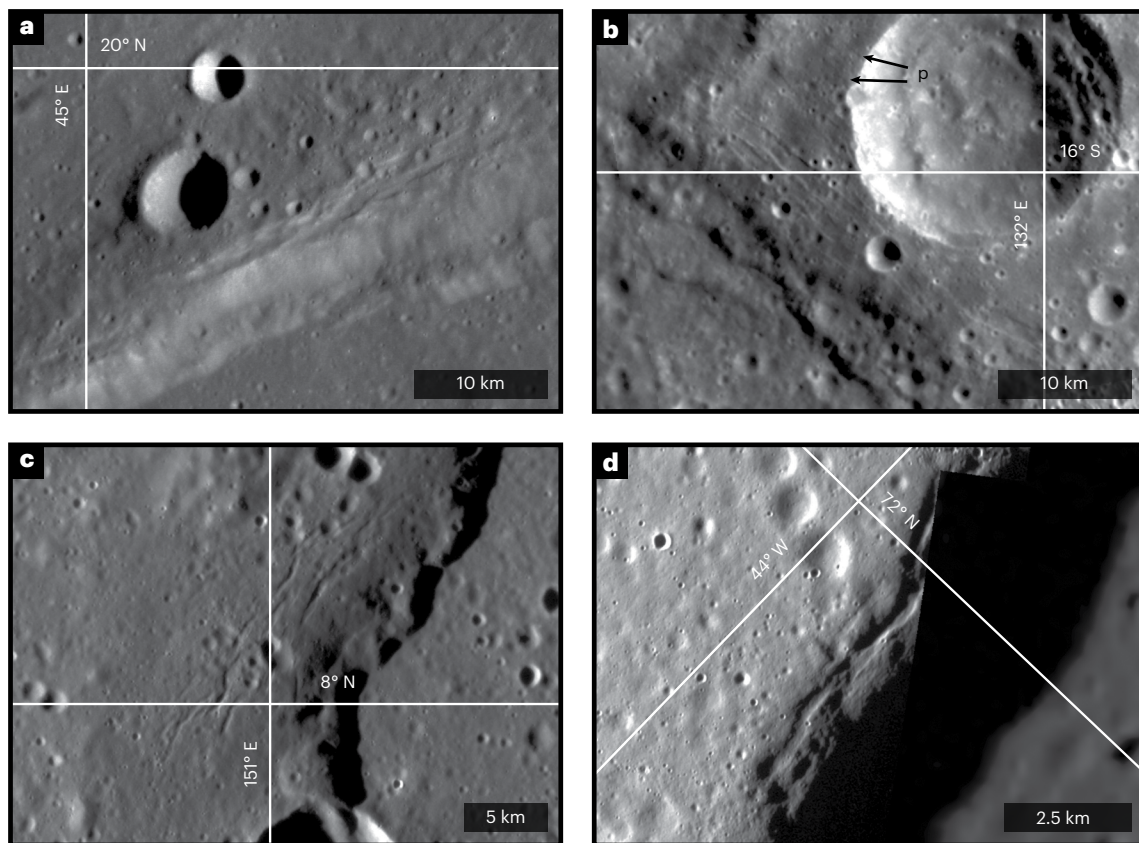
Fig. 1 | Examples of 'certain' grabens. a, Calypso Rupes (image frame EN1014011971M) with some of the largest certain grabens on Mercury. **b,c**, Alpha Crucis Rupēs (image frames EN0231136925M, EN0231136927M and EN0231136960M; **b**) and Alvin Rupes (image frame EN1015167012M; **c**) with horsts and grabens near the crest of the fold; black arrows and 'p' identify additional 'probable' grabens. **d**, Zapiola Rupes (image frames EN1052963740M and EN1052963743M overlain on H01 HIW mosaic) with examples of some of the smallest and shallowest certain grabens on Mercury. More examples are available in Extended Data Figs. 1–5. Credit: MESSENGER images from NASA/JHUAPL/CIW.

predicted rate of infilling. Consequently, we provide substantial evidence of widespread, geologically recent tectonic activity on Mercury.

Grabens and their distribution

A graben is a down-dropped block of material bordered by parallel normal faults. The grabens in this investigation (Figs. 1–3, Extended Data Figs. 1–5 and Supplementary Data 1) were probably formed by local tensional stresses that developed because of continued strain of a larger parent shortening structure. Grabens such as we report are theorized to have formed in response to anticlinal folding in the back-scarp region[16]. Individual graben morphology is probably controlled by local regolith and surface material properties. Grabens can occur singly or in subparallel groups separated by upstanding horsts. The texturally sharp nature of these small, shallow grabens shows that they are young surface structures. We categorized the grabens (Figs. 2 and 3) on the basis of our certainty in their identification. In total, there are 727 grabens, of which we identify 190 as 'certain' (Figs. 2 and 3 and Supplementary Data 1).

The certain grabens are widely distributed (Figs. 2 and 3, Extended Data Fig. 6 and Supplementary Data 1). They can be found in 13 out of 15 of Mercury's mapping quadrangles (Fig. 2c), from 72° N to 76° S, and occur on 48 individual shortening structures, forming a dataset comprising 131 digitized lines. Another 244 structures host 'probable' grabens (Figs. 2 and 3 and Supplementary Data 1). It is likely that many, or even most, of these probable grabens are real, but the current image quality is insufficient for us to be certain in any individual case. We therefore base our analysis and conclusions solely on certain grabens.

Examples of all types of shortening structures (lobate scarps, wrinkle ridges and high-relief ridges) display superposed grabens, but of the 48 shortening structures hosting certain grabens, lobate scarps are most common (97%). The parent shortening structures cut all plains materials and craters, can be basin bounding and vary in length (10s to 1,000s of kilometres) and relief (10s of metres to a few kilometres) (Fig. 3 and Extended Data Fig. 6). Our documentation of so many grabens is important in two respects: for such small features to still be visible demonstrates that they must be young, and their distribution shows that this recent tectonism is widespread.

To consider first the spatial distribution of grabens on shortening structures (Figs. 2 and 3 and Supplementary Data 1), certain grabens are absent in only H05 and H07 (Fig. 2c). Notably, there is a concentration of certain grabens in the equatorial quadrangles H08, H09 and H10, with 65% of all certain grabens in H08 and H09, which encompass the south circum-Caloris region. This region is predominantly smooth volcanic plains[22,23], and the tectonic structures cutting these plains have the clearest and most conspicuous examples of grabens on Mercury (Extended Data Figs. 1–5 and Supplementary Data 1 and 2). The concentration of grabens in this region is almost certainly related to the Caloris basin. Post-impact isostatic readjustment[24] of the crust and subsequent loading by volcanic plains may have promoted tectonic structures propagating in this region[25]. Of note, ~42% (81 out of 190) of all certain grabens occur in this region, on ~29% (14 out of 48) of the associated shortening structures, and these 14 structures strike radially from the rim of the Caloris basin, with a majority in the south circum-Caloris region.
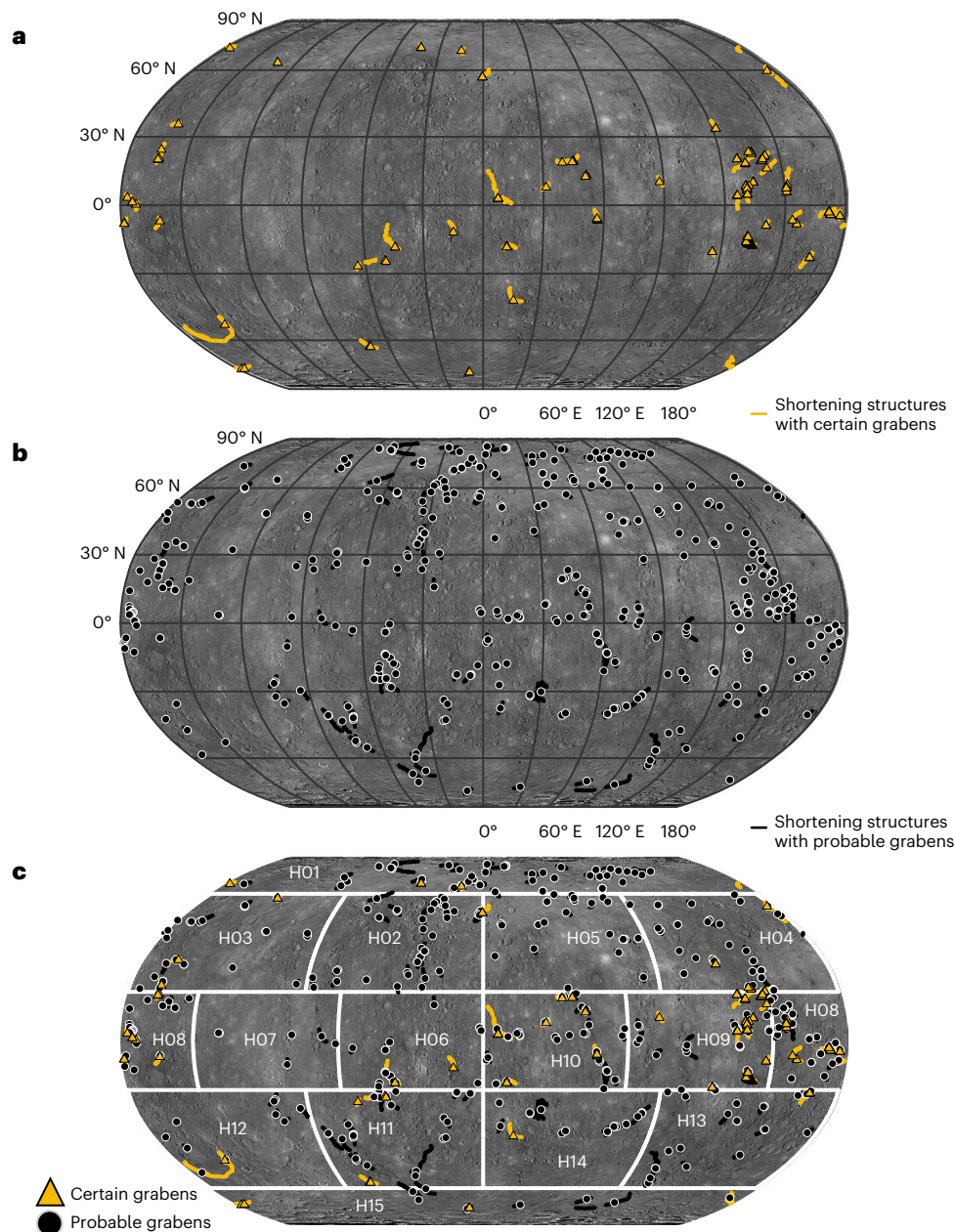
Fig. 2 | Global maps of certain and probable grabens. a, Certain grabens and parent shortening structures. **b**, Probable grabens and parent shortening structures. **c**, Quadrangle map showing certain and probable grabens with their respective parent shortening structures. Credits: MDIS global monochrome basemap from ref. 18; MESSENGER images from NASA/JHUAPL/CIW.

Length, depth and age of grabens

The texturally sharp morphology of the grabens we have identified suggests these are very young features compared with most landforms on Mercury. To further demonstrate that the grabens are geologically young, we undertook shadow measurements of all certain grabens covered by NAC frames that have measurable shadows. This allowed us to estimate the depths of the grabens and compare them with terrestrial and lunar analogues. We were able to make 331 shadow-based depth calculations for 99 of the certain grabens on 29 of 48 shortening structures (Extended Data Fig. 7 and Supplementary Data 3). Of the 331 measurements, 220 were less than 50 m deep, 92 were 50–100 m deep and 19 were >100 m deep.

The age of each graben can be estimated on the basis of an assumed rate of infilling and an estimated original graben depth. Original graben depth was estimated as being equivalent to the maximum displacement

of the normal faults bounding the graben, which in turn is related to the fault length. Fault length is influenced primarily by the tectonic regime and mechanical properties of the material being deformed[26,27]. The relationship between maximum displacement and the fault length can be expressed as

$$D_{max} = \gamma L^n \tag{1}$$

where D_{max} is the maximum displacement, γ is the scaling factor and L is the fault length. The approximation $n = 1$ has been shown to be valid for terrestrial[26,28] and lunar[27,29,30] populations. Fault population γ values are distributed around ~1.0×10^{-2}, with maximum variation in γ value of 1.0×10^{-1} to 1.0×10^{-3} (refs. 26,27).

We measured the lengths of faults bounding the grabens and plotted measured lengths versus average measured depth for the

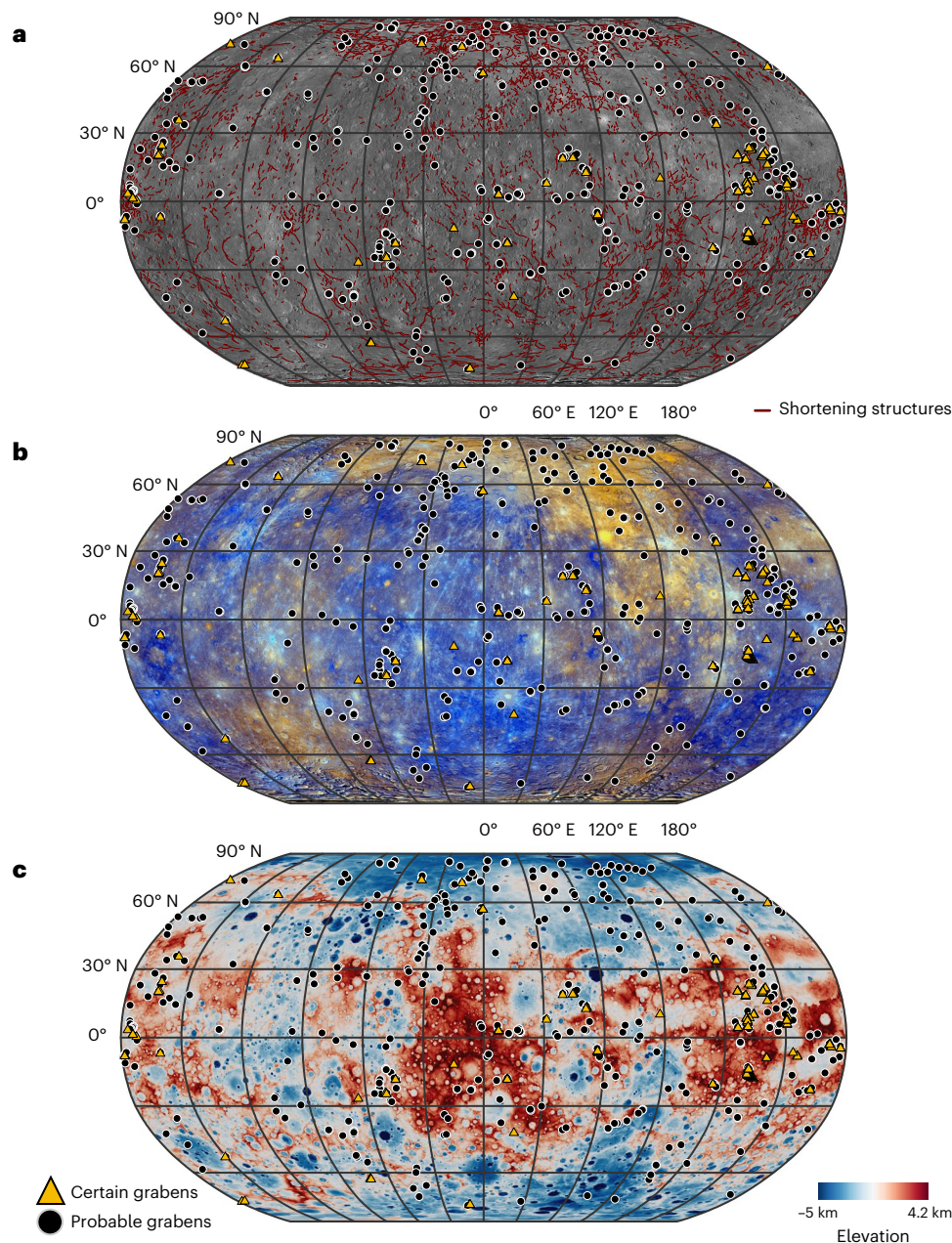**Fig. 3 | Grabens on Mercury. a**, Robinson projection of Mercury with our global map of potential shortening structures (red lines) and associated grabens (see key) overlain on the global monochrome basemap[18]. **b**, MDIS Global Enhanced Color Mosaic[51] overlain on global monochrome basemap with grabens. **c**, MDIS DEM (digital elevation model)[52] overlain on global monochrome basemap with grabens. The global map of grabens and the global map of shortening structures are available in Supplementary Data 1 and 2. Credit: MESSENGER images from NASA/JHUAPL/CIW.

99 certain grabens for which we have shadow measurements (Fig. 4, Extended Data Fig. 7 and Supplementary Data 3). Our data plot almost entirely within the expected γ range of 1.0×10^{-1} and 1.0×10^{-3} but can generally be seen plotting lower than the terrestrial data. The clustering of our data in the middle of the range is best explained by the Hermean grabens following terrestrial and lunar trends in displacement/length and being only slightly infilled. To augment this assessment, it is recognized that displacement/length scales with gravity[31]. Analyses of thrust fault populations for the terrestrial planets show that Mercury and Mars have smaller fault displacement compared with equal-length faults on Earth[31,32]. Although normal fault displacement/length values for Mercury have only been predicted, not measured[31] (Fig. 4, Predicted displacement/length for Mercury normal faults[31]), the observation that most of our data plot lower in the displacement/length field than the

terrestrial studies supports this prediction (although our data do still plot mostly above the predicted Hermean trend line). The datapoints with very low displacement for a given length could indicate examples of older grabens that have undergone more infilling or were simply shallow when formed. This evidence collectively suggests that most of the grabens are geologically recent: if they were not, their measured depths would tend to be shallow compared with their displacement inferred from their lengths, and they would plot very much lower in the displacement/length field.

We made quantitative estimates of the age of each graben by calculating the time taken for each graben to be filled from its original to its present depth, assuming the original depth followed the terrestrial/ lunar displacement/length relationship with $\gamma = 1 \times 10^{-2}$ and applying a suitable infill rate. Infill rate can be derived from studies of lunar
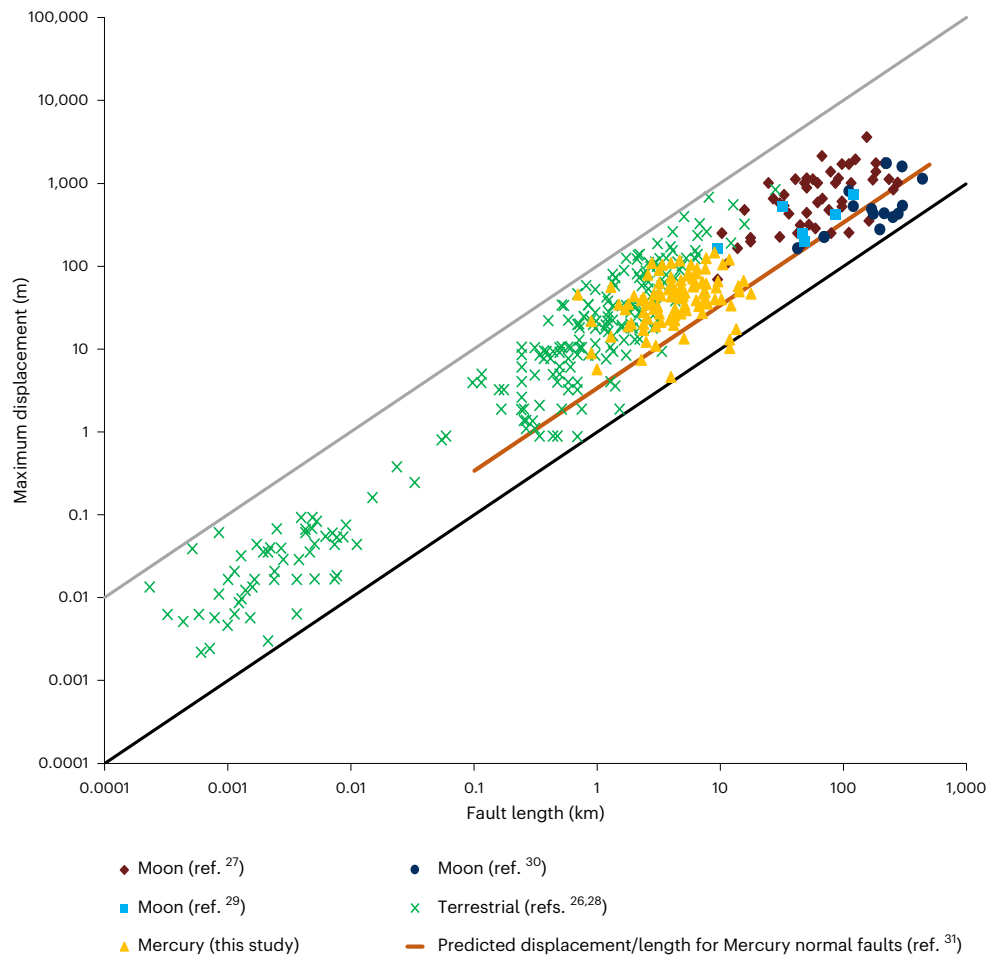
Fig. 4 | Displacement/length scaling of Mercury grabens compared with terrestrial normal faults and lunar grabens. Mercury data are for all measurable certain grabens associated with large-scale shortening structures. Other data from ref. 27.

boulder tracks measured in Apollo 17 images[16,33,34]. The infilling of shallow depressions on the Moon is estimated as 5± cm Ma^{-1} (ref. 34). We apply this rate as a conservative estimate. However, Mercury has a substantially thicker regolith[35,36] compared with the Moon due to a greater regolith production rate[37]. Mercury also has a higher micrometeoric flux[38–40]; hence, increased abrasion of surface features by micrometeoric impactors is expected[41]. It is accepted that craters on Mercury degrade at least twice as fast as craters of the same size on the Moon on the basis of topographic diffusivity measurements[42,43]; however, this rate of degradation could be increased further still if predictions of a Hermean nonporous crust hold true[42]. With consequential increased rate of infilling and erasure of Hermean surface features (such as grabens) by impact gardening and topographic diffusion, we doubled the lunar 5± cm Ma^{-1} rate and applied an infill rate of 10 ± 6 cm Ma^{-1} to more realistically represent the degradation rate for Mercury.

For some grabens, the measured shadow depth was greater than the inferred original depth from equation (1) when $\gamma = 1 \times 10^{-2}$, suggesting either that there was no infill and therefore a very young age or that these examples are simply deeper than typical. For the remaining grabens, assuming maximum lunar and Hermean infilling rates of 8 cm Ma^{-1} and 16 cm Ma^{-1}, respectively, ages of ≤230 Ma to ≤120 Ma were calculated. Varying γ such that 95% of the measured graben depths are less than the inferred original depth gives $\gamma = 2.9 \times 10^{-2}$ and median ages of <1,100 Ma to <550 Ma for the grabens. These calculations demonstrate that if these grabens on Mercury follow similar displacement/length relationships to those on Earth and on the Moon, then they must be young features, many of them having formed in the past few 100 Ma.

Discussion

The continued activity of tectonic structures on Mercury resulting from secular cooling has been predicted[16,44–47]; the evidence provided here in the form of small grabens confirms this. Furthermore, this geologically recent activity is widespread, supporting thermochemical evolution models for Mercury in which cooling of the interior is slow[3,45], resulting in prolonged global contraction. The presence of a thick megaregolith[3] in addition to a theorized liquid FeS layer encompassing a silicon-bearing core[48] and inefficient mantle convection[45] or cessation of mantle convection[44,46,49] could all contribute to Mercury's thermal insulation, considerably slowing the cooling and subsequent contraction of the planet. The detection of high numbers of grabens around the Caloris Basin, particularly within smooth volcanic plains exterior to the basin, is important as it supports the theory of a regionally thin crust and subsequently a thin elastic lithosphere that could have promoted flexure and subsidence in this region[3]. Furthermore, the population of grabens around Caloris provides further input into thermochemical evolution models, which will need to account for how this very large impact has affected or is still affecting Mercury's evolution.

The MESSENGER spacecraft's highly elliptical orbit resulted in a contrast of image spatial resolution between the northern and southern hemispheres. If we compare the number of NAC frames that we analysed (150 m pixel^{-1} or better) from the two poles (Extended Data Fig. 8), there were 4,174 frames intersecting tectonic structures for H01 and only 153 for H15 (both counts include frames that overlap with adjacent quadrangles). It is therefore important to understand that data availability and resolution are the major limitations of this

investigation. We expect that the improved image data resolution and coverage that will be provided by the BepiColombo spacecraft[50], which will enter orbit around Mercury in 2025, will mean many more of these landforms will be confirmed or discovered. Analysis of that dataset will help better constrain models of Mercury's evolution by better measuring the population and spatial distribution of these recent tectonic features.

Online content

Any methods, additional references, Nature Portfolio reporting summaries, source data, extended data, supplementary information, acknowledgements, peer review information; details of author contributions and competing interests; and statements of data and code availability are available at https://doi.org/10.1038/s41561-023-01281-5.

References

1. Solomon, S. C., McNutt, R. L., Gold, R. E. & Domingue, D. L. MESSENGER mission overview. *Space Sci. Rev.* **131**, 3–39 (2007).
2. Byrne, P. K. et al. Mercury's global contraction much greater than earlier estimates. *Nat. Geosci.* **7**, 301–307 (2014).
3. Watters, T. R. A case for limited global contraction of Mercury. *Commun. Earth Environ.* **2**, 9 (2021).
4. Melosh, H. J. Global tectonics of a despun planet. *Icarus* **31**, 221–243 (1977).
5. Matsuyama, I. & Bills, B. G. Global contraction of planetary bodies due to despinning: application to Mercury and Iapetus. *Icarus* **209**, 271–279 (2010).
6. Keane, J. T. & Matsuyama, I. True polar wander of Mercury. In *Proceedings of the Conference on Mercury: Current and Future Science of the Innermost Planet*, LPI contribution no. 2047, id.6098 (Lunar and Planetary Institute, 2018).
7. King, S. D. Pattern of lobate scarps on Mercury's surface reproduced by a model of mantle convection. *Nat. Geosci.* **1**, 229–232 (2008).
8. Dombard, A. J. & Hauck, S. A. Despinning plus global contraction and the orientation of lobate scarps on Mercury: predictions for MESSENGER. *Icarus* **198**, 274–276 (2008).
9. Watters, T. R. & Nimmo, F. in *Planetary Tectonics* (eds Watters, T. R. & Schultz, R. A.) 15–80 (Cambridge Univ. Press, 2010); https://doi.org/10.1017/CBO9780511691645.003
10. Strom, R. G., Trask, N. J. & Guest, J. E. Tectonism and volcanism on Mercury. *J. Geophys. Res.* **80**, 2478–2507 (1975).
11. Watters, T. R., James, P. B. & Selvans, M. M. Mercury's crustal thickness and contractional strain. *Geophys. Res. Lett.* **48**, e2021GL093528 (2021).
12. Banks, M. E. et al. Duration of activity on lobate-scarp thrust faults on Mercury. *J. Geophys. Res. Planets* **120**, 1751–1762 (2015).
13. Byrne, P. K. Tectonism of Mercury. in *Oxford Research Encyclopedia of Planetary Science* (eds Read, P. et al.) 1–38 (Oxford Univ. Press, 2019); https://doi.org/10.1093/acrefore/9780190647926.013.128
14. Tosi, N. & Padovan, S. in *Mantle Convection and Surface Expressions* (eds Marquardt, H. et al.) 455–489 (AGU and Wiley, 2021); https://doi.org/10.1002/9781119528609.ch17
15. Klimczak, C., Byrne, P. K., Şengör, A. M. C. & Solomon, S. C. Principles of structural geology on rocky planets. *Can. J. Earth Sci.* **56**, 1437–1457 (2019).
16. Watters, T. R. et al. Recent tectonic activity on Mercury revealed by small thrust fault scarps. *Nat. Geosci.* **9**, 743–747 (2016).
17. Byrne, P. K., Klimczak, C. & Celâl Şengör, A. M. in *Mercury: The View after Messenger* (eds Solomon, S. C. et al.) 249–286 (Cambridge Univ. Press, 2018); https://doi.org/10.1017/9781316650684.011
18. Hawkins, S. E. et al. The Mercury Dual Imaging System on the MESSENGER spacecraft. *Space Sci. Rev.* **131**, 247–338 (2007).
19. Melosh, H. J. & McKinnon, W. B. The tectonics of Mercury. in *Mercury* (eds Vilas, F. et al.) 374–400 (University of Arizona Press, 1988); https://ui.adsabs.harvard.edu/abs/1988merc.book..374M/abstract
20. Wright, J., Rothery, D. A., Balme, M. R. & Conway, S. J. Constructional volcanic edifices on Mercury: candidates and hypotheses of formation. *J. Geophys. Res. Planets* **123**, 952–971 (2018).
21. Barnouin, O. S. et al. The morphology of craters on Mercury: results from MESSENGER flybys. *Icarus* **219**, 414–427 (2012).
22. Rothery, D. A., Mancinelli, P., Guzzetta, L. G. & Wright, J. Mercury's Caloris Basin: continuity between the interior and exterior plains. *J. Geophys. Res. Planets* **122**, 560–576 (2017).
23. Denevi, B. W. et al. The distribution and origin of smooth plains on Mercury. *J. Geophys. Res. Planets* **118**, 891–907 (2013).
24. Kennedy, P. J., Freed, A. M. & Solomon, S. C. Mechanisms of faulting in and around Caloris Basin, Mercury. *J. Geophys. Res. Planets* **113**, 1–12 (2008).
25. Klimczak, C., Kling, C. L. & Byrne, P. K. Topographic expressions of large thrust faults on Mars. *J. Geophys. Res. Planets* **123**, 1973–1995 (2018).
26. Cowie, P. A. & Scholz, C. H. Displacement-length scaling relationship for faults: data synthesis and discussion. *J. Struct. Geol.* **14**, 1149–1156 (1992).
27. Martin, E. S. & Watters, T. R. Displacement-length scaling relations of nearside graben: evidence of restricted normal faults on the Moon. *Icarus* **388**, 115215 (2022).
28. Watters, T. R., Schultz, R. A. & Robinson, M. S. Displacement length relations of trust faults associated with lobate scarps on Mercury and Mars comparison with terrestrial faults. *Geophys. Res. Lett.* **27**, 3659–3662 (2000).
29. Watters, T. R. & Johnson, C. L. in *Planetary Tectonics* (eds Watters, T. R. & Schultz, R. A.) 121–182 (Cambridge Univ. Press, 2010).
30. Callihan, M. B. & Klimczak, C. Topographic expressions of lunar graben. *Lithosphere* **11**, 294–305 (2019).
31. Schultz, R. A., Okubo, C. H. & Wilkins, S. J. Displacement-length scaling relations for faults on the terrestrial planets. *J. Struct. Geol.* **28**, 2182–2193 (2006).
32. Atkins, R. M., Byrne, P. K., Bohnenstiehl, D. R. & Wegmann, K. W. A morphometric investigation of large-scale crustal shortening on Mars. *J. Geophys. Res. Planets* **127**, e2021JE007110 (2022).
33. Watters, T. R., Robinson, M. S., Banks, M. E., Tran, T. & Denevi, B. W. Recent extensional tectonics on the Moon revealed by the Lunar Reconnaissance Orbiter Camera. *Nat. Geosci.* **5**, 181–185 (2012).
34. Arvidson, R., Drozd, R. J., Hohenberg, C. M., Morgan, C. J. & Poupeau, G. Horizontal transport of the regolith, modification of features, and erosion rates on the lunar surface. *Moon* **13**, 67–79 (1975).
35. Kreslavsky, M. A. & Head, J. W. A thicker regolith on Mercury. In *Proc. 46th Lunar and Planetary Science Conference*, abstr. 1246 (Lunar and Planetary Institute, 2015).
36. Kreslavsky, M. A., Head, J. W., Neumann, G. A., Zuber, M. T. & Smith, D. E. Kilometer-scale topographic roughness of Mercury: correlation with geologic features and units. *Geophys. Res. Lett.* **41**, 8245–8251 (2014).
37. Kreslavsky, M. A., Zharkova, A. Y., Head, J. W. & Gritsevich, M. I. Boulders on Mercury. *Icarus* **369**, 114628 (2021).
38. Cintala, M. J. Impact-induced thermal effects in the lunar and Mercurian regoliths. *J. Geophys. Res.* **97**, 947–973 (1992).
39. Borin, P., Cremonese, G., Marzari, F., Bruno, M. & Marchi, S. Statistical analysis of micrometeoroids flux on Mercury. *Astron. Astrophys.* **503**, 259–264 (2009).
40. Marchi, S. et al. Global resurfacing of Mercury 4.0–4.1 billion years ago by heavy bombardment and volcanism. *Nature* **499**, 59–61 (2013).
41. Zharkova, A. Y., Kreslavsky, M. A., Head, J. W. & Kokhanov, A. A. Regolith textures on Mercury: comparison with the Moon. *Icarus* **351**, 113945 (2020).

42. Fassett, C. I. et al. Evidence for rapid topographic evolution and crater degradation on Mercury from simple crater morphometry. *Geophys. Res. Lett.* **44**, 5326–5335 (2017).

43. Du, J. et al. Thickness of lunar mare basalts: new results based on modeling the degradation of partially buried craters. *J. Geophys. Res. Planets* **124**, 2430–2459 (2019).

44. Hauck, S. A., Dombard, A. J., Phillips, R. J. & Solomon, S. C. Internal and tectonic evolution of Mercury. *Earth Planet. Sci. Lett.* **222**, 713–728 (2004).

45. Grott, M., Breuer, D. & Laneuville, M. Thermo-chemical evolution and global contraction of Mercury. *Earth Planet. Sci. Lett.* **307**, 135–146 (2011).

46. Tosi, N., Grott, M., Plesa, A. C. & Breuer, D. Thermochemical evolution of Mercury's interior. *J. Geophys. Res. Planets* **118**, 2474–2487 (2013).

47. Crane, K. T. & Klimczak, C. Timing and rate of global contraction on Mercury. *Geophys. Res. Lett.* **44**, 3082–3089 (2017).

48. Pommier, A., Leinenweber, K. & Tran, T. Mercury's thermal evolution controlled by an insulating liquid outermost core? *Earth Planet. Sci. Lett.* **517**, 125–134 (2019).

49. Michel, N. C. et al. Thermal evolution of Mercury as constrained by MESSENGER observations. *J. Geophys. Res. Planets* **118**, 1033–1044 (2013).

50. Rothery, D. A. et al. Rationale for BepiColombo studies of Mercury's surface and composition. *Space Sci. Rev.* **216**, 66 (2020).

51. Denevi, B. W. et al. Calibration, projection, and final image products of MESSENGER's Mercury Dual Imaging System. *Space Sci. Rev.* **214**, 2 (2018).

52. Becker, K. J. et al. First global digital elevation model of Mercury. In *Proc. 47th Lunar and Planetary Science Conference*, abstr. 2959 (Lunar and Planetary Institute, 2016).

Methods

Data

To produce the global shortening structure map (Fig. 3a and Supplementary Data 2) for the primary basemap we used the MESSENGER version 1.0 monochrome, moderate solar incidence angle (~74°) Map-Projected Basemap Reduced Data Record. This global mosaic has a resolution of ~166 m pixel^{-1} (256 pixels per degree) and was used alongside ancillary MDIS data products: monochrome high-incidence-angle (~78°) tiles (~166 m pixel^{-1}) and the Mercury Laser Altimeter and stereo-derived DEMs[52]. These products were sourced from the Planetary Data System Cartography and Imaging Sciences Node. For the grabens survey, we used NAC frames obtained from the Mercury Orbital Data Explorer as part of the NASA (National Aeronautics and Space Administration) Planetary Data System Geosciences node. We processed all data using the United States Geological Survey ISIS3 (Integrated Software for Imagers and Spectrometers version 3) to produce map-projected data for ingestion into ArcGIS for analysis.

Tectonic mapping

We have examined and built upon previous tectonic map databases[2,3] to produce a global map of potential shortening structures to use as a methodological tool for our global grabens survey. Our mapping was undertaken to improve the accuracy of linework and because previous databases either did not have end-of-mission data products available at the time of completion[2] or did not map all compressional tectonic structures[3]. To produce a global map of shortening structures at the highest resolution and completeness, we used the latest available data products to map all resolvable structures at a constant 1:500,000 drafting scale. We recognize and interpret all thrust fault-related structures on the basis of their morphology. Positive relief landforms with a recognizable break in slope are interpreted as surface-breaking thrust faults (lobate scarps), with a steep escarpment representing the leading edge and vergence of the underlying thrust. Typically, these structures are asymmetrical in profile with a gently sloping back limb and exhibit linear to arcuate map patterns, characteristic of thrust fault systems[15,25]. We also mapped wrinkle ridges—antiformal ridges that are archetypically symmetrical in profile but are often observed as asymmetrical. These structures are interpreted as folding produced by a blind thrust[15]. For lobate scarps, polylines were drawn along the leading edge of a structure where a sharp break in slope is discernible. For wrinkle ridges, lines were drawn along the mid-line of a ridge. For high-relief ridges, the comprising lobate scarp(s) were mapped individually. A vertex was placed every 2,000 m using ArcGIS's streaming tool. We have not mapped all shortening structures within the Caloris basin as probable basin-related structures are not of interest to this investigation. Only structures that cut the rim of the Caloris basin or are part of a sequence of thrusts that cross-cut the rim of the basin were digitized.

Graben survey

For the global grabens survey, we first selected all NAC frames 150 m pixel^{-1} or better that intersected any of the potential shortening structures in our database. To do this, we used a combination of Java Mission Planning and Analysis for Remote Sensing[53] and ArcGIS Pro to first query and then filter the 93,408 NAC frames of which 25,489 intersected the tectonic structures that we mapped. We then downloaded and processed the intersecting images in ISIS3 where spacecraft and camera information, radiometric calibration, map projection and photometric corrections were made so that the images could be analysed in ArcGIS. On a quadrangle-by-quadrangle basis, we inspected all the NAC images for each of the tectonic structures in context, superposed on the basemap. We identified grabens on the basis of their morphology: linear to sublinear mostly flat-floored depressions bounded on two sides by parallel to subparallel escarpments, sometimes found either side of horsts, raised fault-bounded blocks that share an escarpment with an adjacent graben or grabens. Once a graben was identified, a point was placed in the centre of the graben. A qualitative certain designation was given to a graben when a structure was obviously noticeable in images whereas a probable designation was given when a structure was perceptible (exhibiting a graben-like morphology, found on top of a shortening structure and parallel to subparallel to the strike of this parent structure but blurred and/or difficult to make out). To avoid misidentifying non-tectonic structures, such as catenae, which can appear graben-like, we took morphology into account and looked for individual crater septa within the depression or an undulating floor to distinguish catenae. When catenae may have been infilled by lavas or impact melt, the orientation of the landform was investigated to ascertain the provenance of the material that could have made the depression by identifying large impacts and other clusters or catenae that share a common orientation and source.

Shadow measurements

To determine the depth of the grabens, we used the well-established shadow-length calculations employed by numerous authors[20,21,54,55] and outlined in Extended Data Fig. 7. Using the highest-resolution NAC frames where there were sufficient shadows to be measured, first a construction line was drawn as the strike of the graben on the rim of the flank that was casting the shadow. A measurement line was then drawn from the construction line in the exact opposite direction of the solar azimuth of the NAC frame. This measurement line was drawn to the edge of the umbral shadow, giving a shadow length. To account for where the Sun was in respect to the spacecraft when it took the image, we applied the following: $\tan i \pm \tan e$, where i is the solar incidence and e is the spacecraft emission angle. A positive emission angle is used in this expression when the spacecraft has taken the image of the surface while looking towards the Sun, and a negative one is used when the Sun is behind the spacecraft[21]. When possible, multiple shadow measurements were taken along the length of the graben, and then the calculated depths were averaged for a final depth result. This was performed to obtain the most robust average depth measurement for each of the grabens. The estimated error for each shadow measurement has been calculated and is found in Supplementary Data 3. The percentage of error per shadow measurement length can be applied to the calculated depth. For ~96% of shadow-length measurements, an error percentage between 0 and 10% has been calculated. With only ~4% ≥10% error, it is unlikely that measurement error has affected our estimates of depth.

Data availability

The MESSENGER data used in this article are available from NASA's Planetary Data System (PDS) Geosciences Node (https://pds-geosciences.wustl.edu/) and the Cartography and Imaging Sciences Node (https://pds-imaging.jpl.nasa.gov/). The datasets produced as part of this study are available in Supplementary Data 1–3 and via Figshare at https://doi.org/10.21954/ou.rd.24167700.v1 (ref. 56).

References

53. Christensen, P. R. et al. JMARS – a planetary GIS. In *Proc. American Geophysical Union Fall Meeting*, abstr. IN22A-06 (American Geophysical Union, 2009).

54. Pike, R. J. Depth/diameter relations of fresh lunar craters: revision from spacecraft data. *Geophys. Res. Lett.* **1**, 291–294 (1974).

55. Chappelow, J. E. & Sharpton, V. L. An improved shadow measurement technique for constraining the morphometry of simple impact craters. *Meteorit. Planet. Sci.* **37**, 479–486 (2002).

56. Man, B., Rothery, D. A., Balme, M. R., Conway, S. J. & Wright, J. Widespread small grabens consistent with recent tectonism on Mercury. *Figshare* https://doi.org/10.21954/ou.rd.24167700.v1 (2023).

Acknowledgements

Author contributions

B.M. led the investigation, undertook data analysis and recorded the study's findings. B.M., D.A.R., M.R.B., S.J.C. and J.W. contributed to scientific discussion and to the writing of the manuscript, and B.M. prepared the figures.

Competing interests

The authors declare no competing interests.

Additional information

Extended data is available for this paper at https://doi.org/10.1038/s41561-023-01281-5.

Supplementary information The online version contains supplementary material available at https://doi.org/10.1038/s41561-023-01281-5.

Correspondence and requests for materials should be addressed to Benjamin Man, David A. Rothery, Matthew R. Balme, Susan J. Conway or Jack Wright.

Peer review information *Nature Geoscience* thanks Chris Okubo, Thomas (Tom) Watters and the other, anonymous, reviewer(s) for their contribution to the peer review of this work. Primary Handling Editors: Tamara Goldin and Stefan Lachowycz, in collaboration with the *Nature Geoscience* team.

**Reprints and permissions information** is available at www.nature.com/reprints.
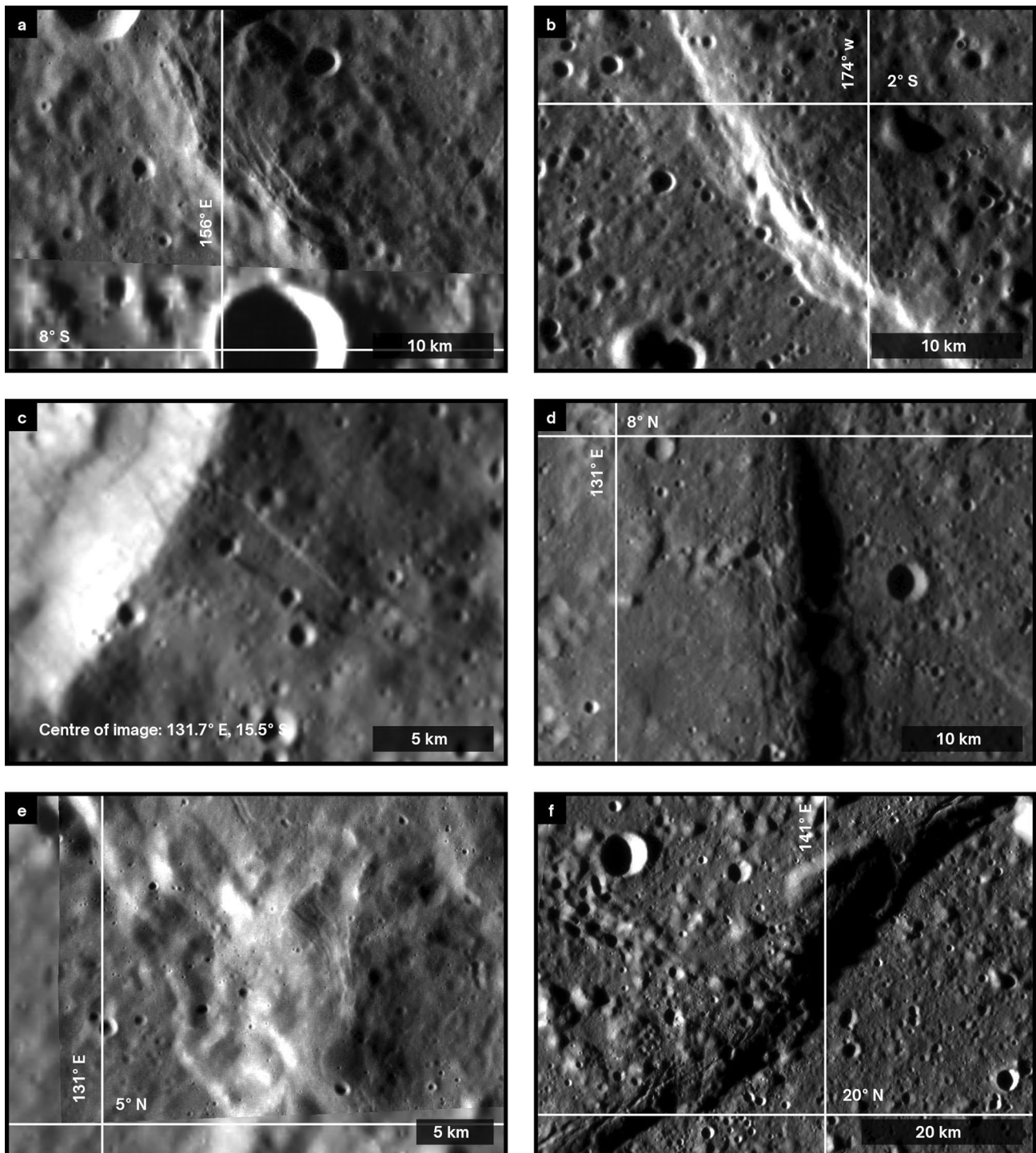
Extended Data Fig. 1 | Examples of grabens 1. a, Protea Rupes (H08) certain (EN0250768612M overlain on MDIS HIW tile), **b**, Tangaroa Rupes (H08) certain (EN1014447282M), **c**, Alpha Crucis Rupēs (H09) certain (EN0251431360M), **d**, (EN1015800736M & EN1015800780M) & **e**, (EN0220807580M overlain on MDIS global BDR mosaic), Arquipelago Rupēs (H09) certain, **f**, Endurance Rupes (H09) certain (EN1015627633M). Credit: MESSENGER images from NASA/JHUAPL/CIW.
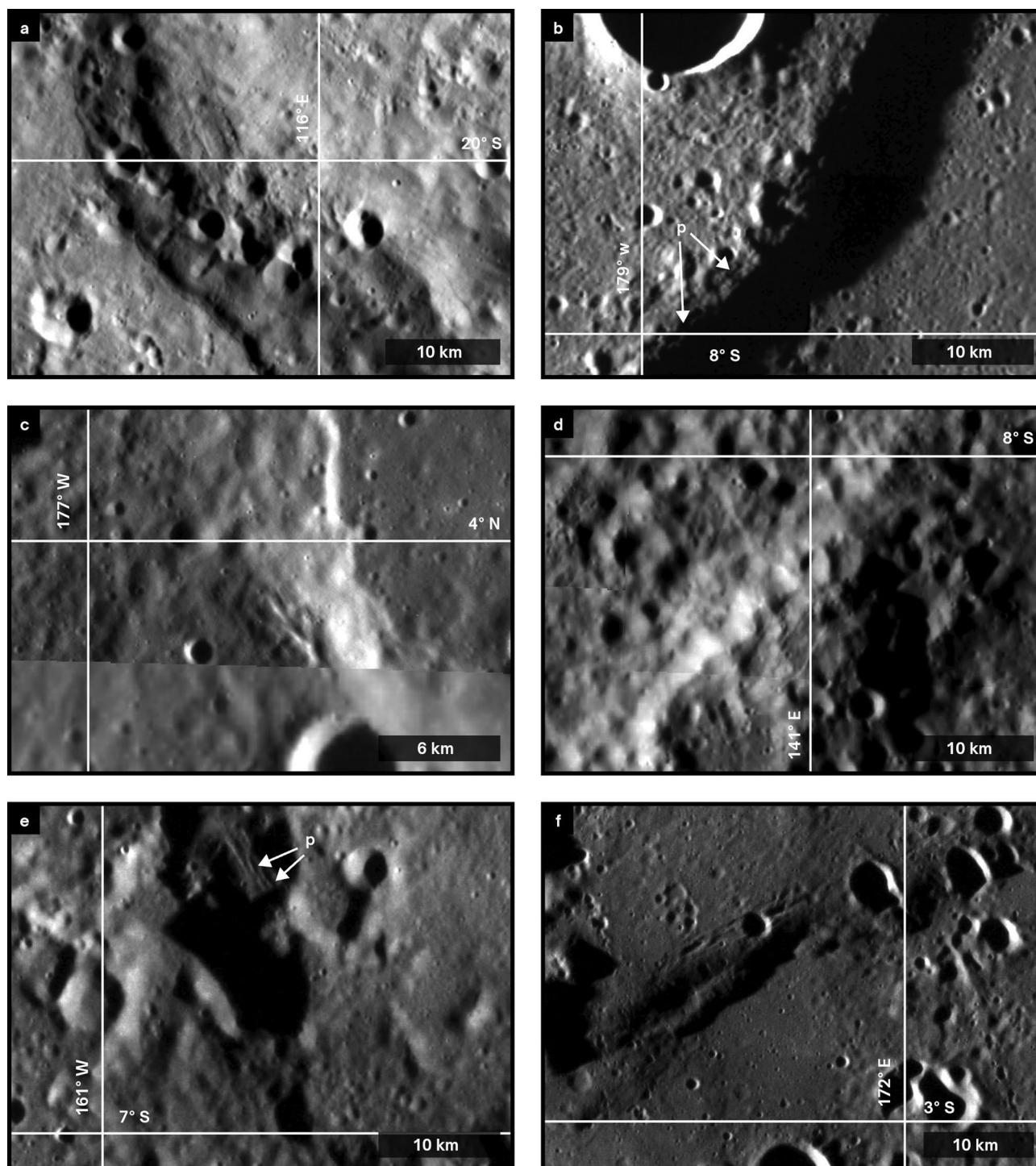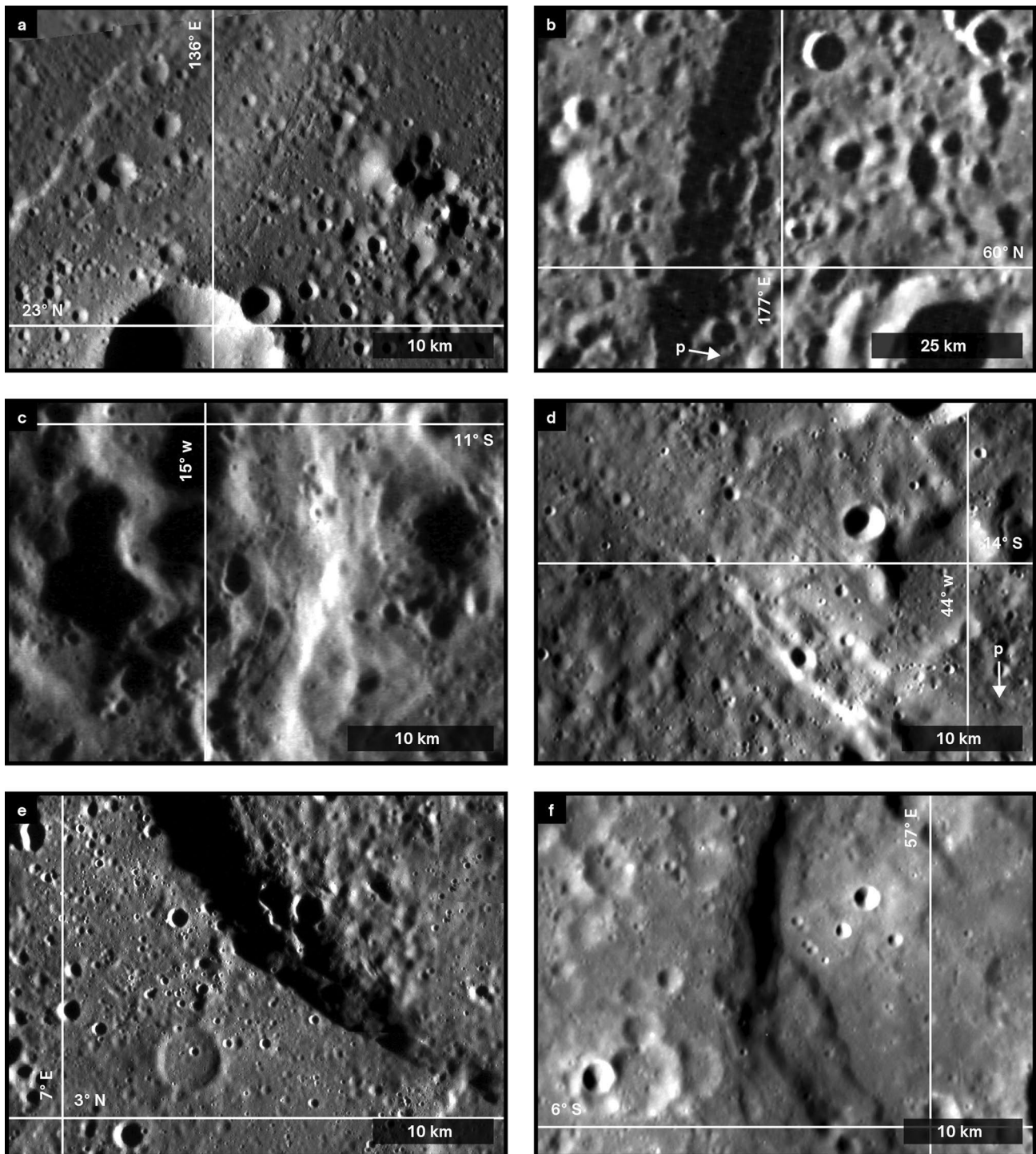
Extended Data Fig. 2 | Examples of grabens 2. a, Astrea Rupes (H09) certain (EN0231353067M & EN0231396273M), **b**, Selen Rupes (H08) certain & probable (MDIS HIW tile), **c**, Unnamed Rupes (H08) certain (EN0258282872M overlain on MDIS global BDR mosaic), **d**, Carrasco Rupēs (H09) certain (EN0236024615M, EN1000274937M & EN1000274876M), **e**, Akademik Rupes (H08) certain & probable (EN0242754192M), **f**, Hesperides Rupes (H08) certain (EN1014792988M). Credit: MESSENGER images from NASA/JHUAPL/CIW.
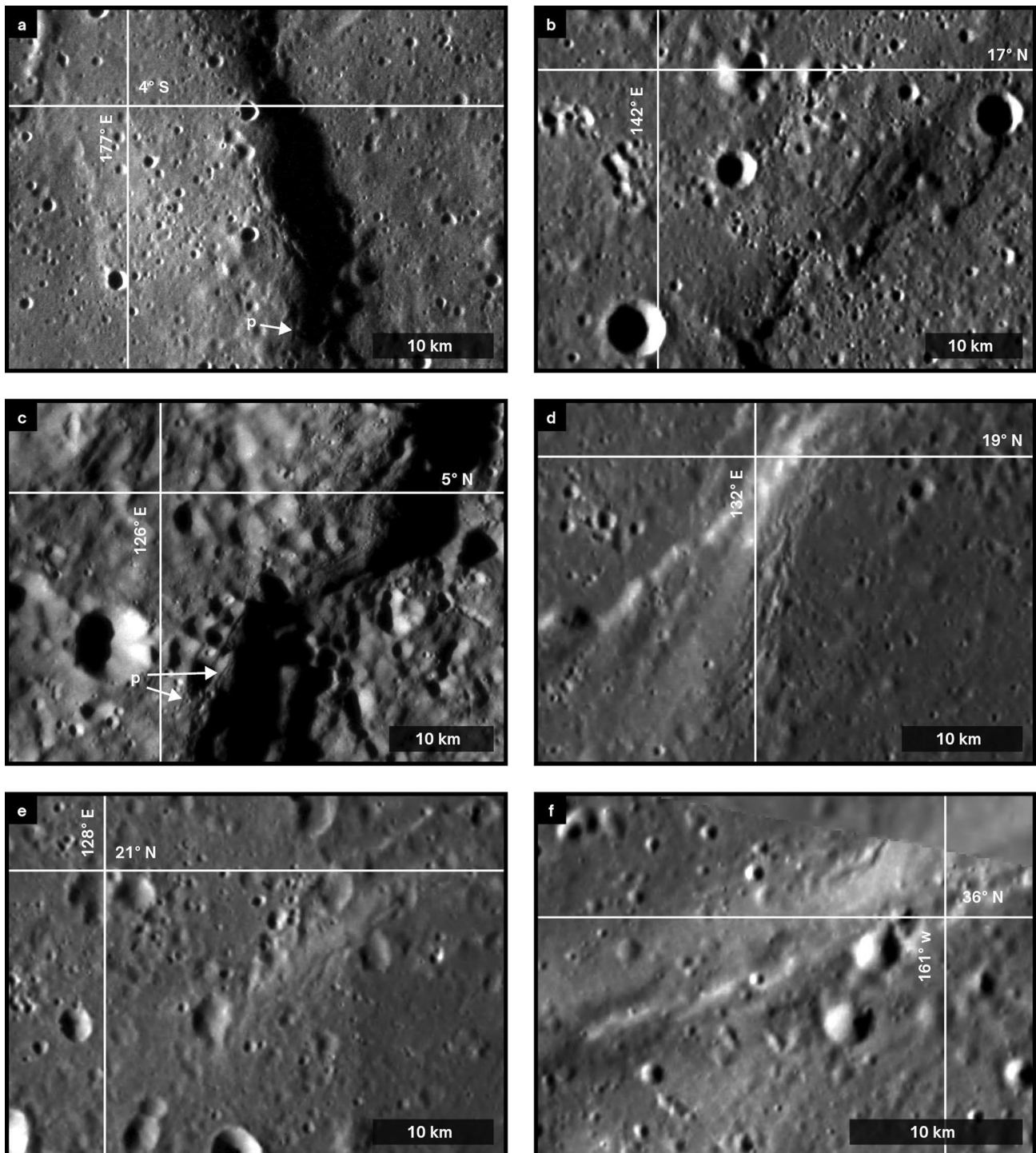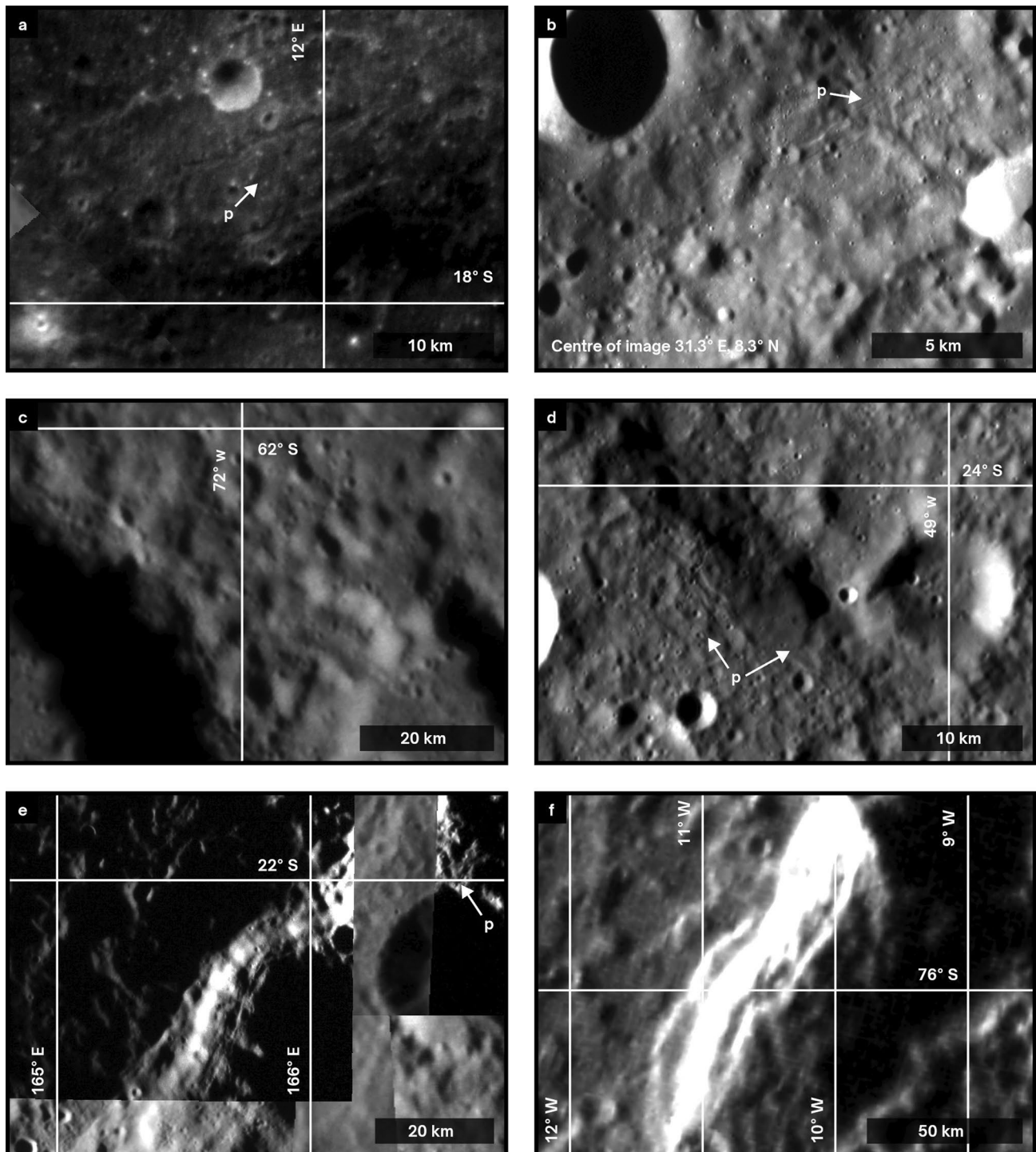
Extended Data Fig. 3 | Examples of grabens 3. a, Lance Rupes (H08) certain & probable (EN1014677849M), **b**, Pelagia Rupes (H09) certain (MDIS HIW tile), **c**, Providencia Rupes (H09) certain & probable (EN1015944874M), **d**, Antares Rupes (H09) certain (MDIS HIW tile), **e**, Unnamed Rupes (H09) certain (MDIS HIW tile), **f**, Vejas Rupes (H03) certain (EN0212502528M overlain on MDIS global BDR mosaic). Credit: MESSENGER images from NASA/JHUAPL/CIW.

Extended Data Fig. 4 | Examples of grabens 4. a, Yelcho Rupes (H04) certain (EN1015541044M, EN1015195383M & EN1015541040M overlain on MDIS global BDR mosaic), **b**, Xue Long Rupes (H04) certain & probable (MDIS global BDR mosaic), **c**, Aegaeo Rupes(H06) certain (EN1015451229M), **d**, Darshak Rupēs (H06) certain & probable (EN0243798227M & EN0243769464M), **e**, Grifo Rupes (H10) certain (EN1014818106M, EN1045296689M, EN1014904474M & EN1014904478M), **f**, Baltica Rupes (H10) certain (EN0239829788M). Credit: MESSENGER images from NASA/JHUAPL/CIW.

Extended Data Fig. 5 | Examples of grabens 5. a, Legend Rupes (H10) certain & probable (EN1004504512M & EN1004359808M overlain on MDIS global BDR mosaic), **b**, Acadia Rupes (H10) certain & probable (EN1029538361M), **c**, Unnamed Rupes (H11) certain (EN0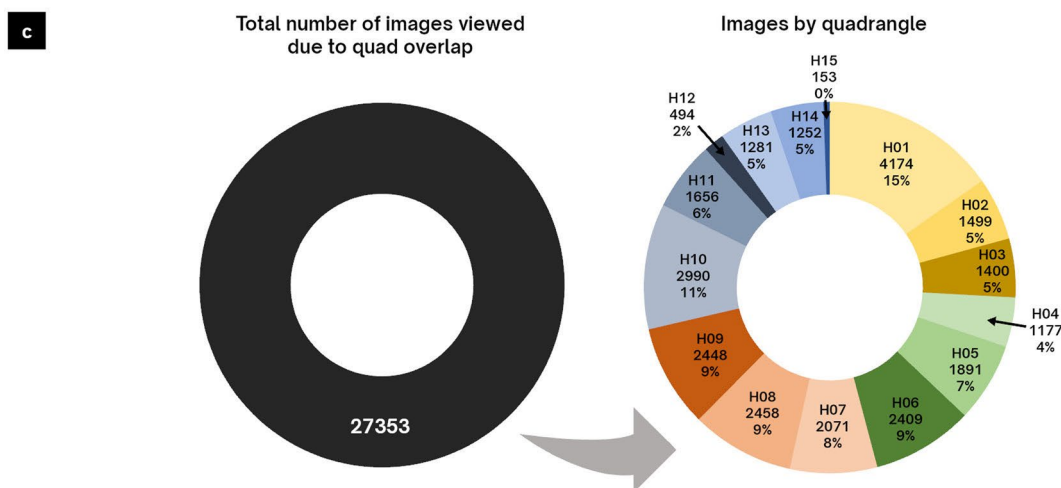223402261M), **d**, Unnamed Rupes (H1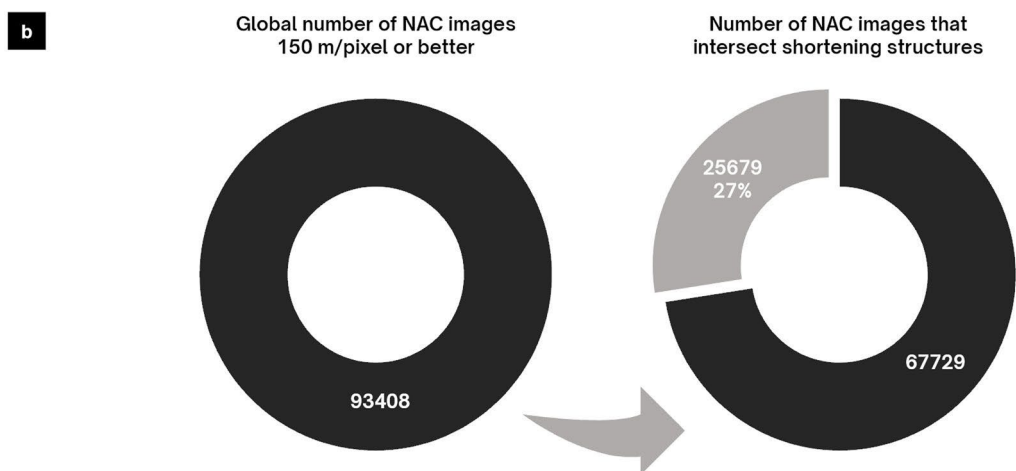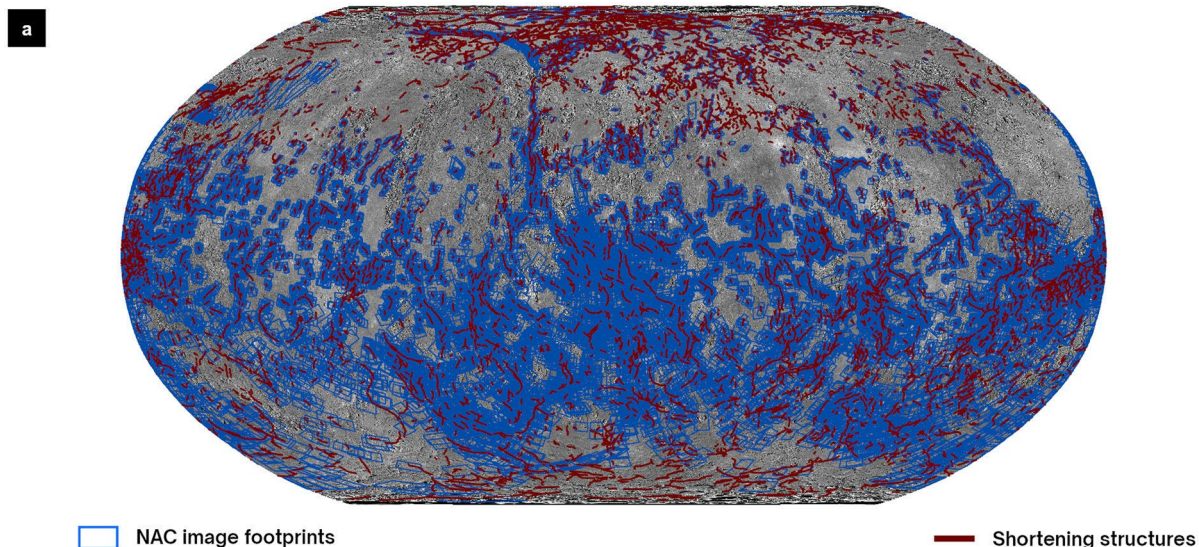1) certain & probable (EN0243884869M), **e**, Unnamed Rupes (H13) certain & probable (EN1015139737M overlain on MDIS HIW tile and global BDR mosaic), **f**, Unnamed Rupes (H15) certain (MDIS HIW tile). Credit: MESSENGER images from NASA/JHUAPL/CIW.
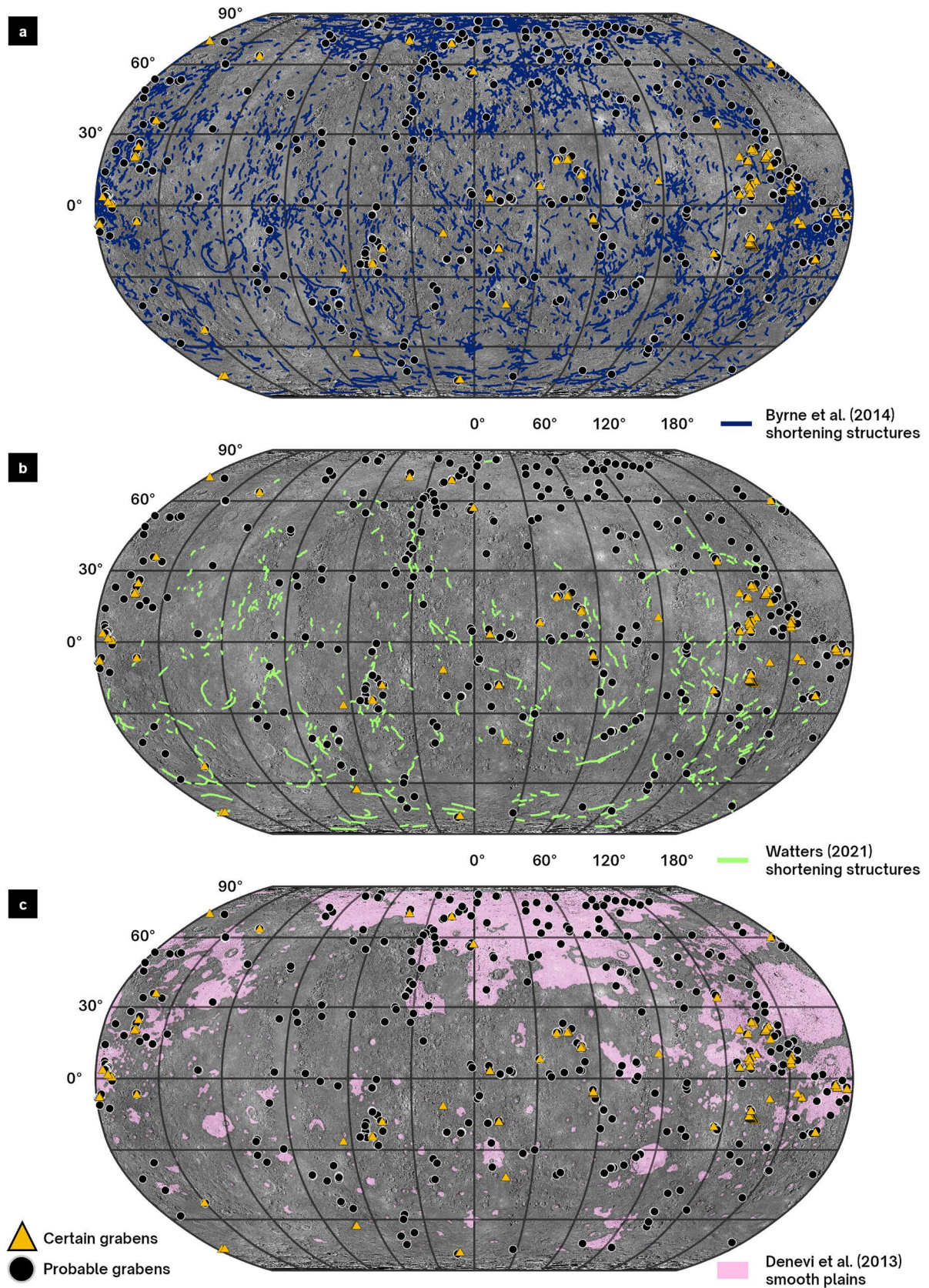
Extended Data Fig. 6 | Published databases with grabens database. a, Data from the shortening structures database of ref. 2. **b**, Data from the shortening structures database of ref. 3. **c**, Data from the smooth plains database of ref. 23. Credit: MESSENGER images from NASA/JHUAPL/CIW.
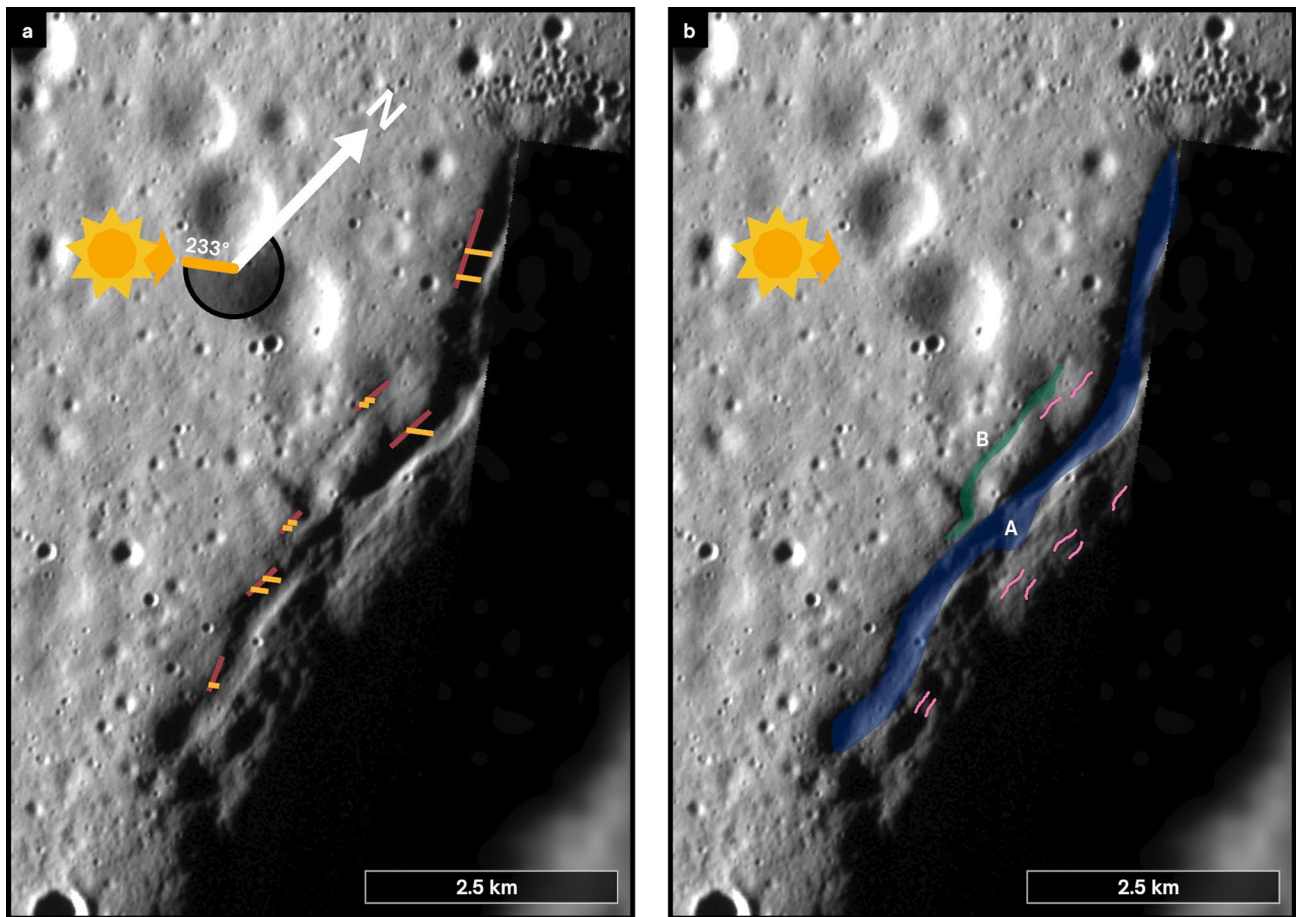
Extended Data Fig. 7 | Shadow measurements diagram. a, Shadow measurements for two grabens. Maroon line = construction line, yellow line = measurement line. Solar Azimuth of NAC frame EN1052963743M = 233°. **b**, Same view with our interpretation, blue area demarcates graben A, green area = graben B, pink lines = tension cracks. Credit: MESSENGER images from NASA/JHUAPL/CIW.

a

NAC image footprints — Shortening structures

b

Global number of NAC images 150 m/pixel or better

93408

Number of NAC images that intersect shortening structures

25679 27%

67729

c

Total number of images viewed due to quad overlap

27353

Images by quadrangle

H15 153 0%
H12 494 2%
H13 1281 5%
H14 1252 5%
H11 1656 6%
H01 4174 15%
H10 2990 11%
H02 1499 5%
H03 1400 5%
H04 1177 4%
H09 2448 9%
H05 1891 7%
H08 2458 9%
H06 2409 9%
H07 2071 8%

Extended Data Fig. 8 | NAC coverage. a, Global map showing NAC image footprint coverage of potential shortening structures overlain on MDIS global BDR mosaic. **b**, Global number of NAC images 150 m/pixel or better that intersect tectonic lineaments. **c**, Number of frames viewed per quadrangle. Credit: MESSENGER images from NASA/JHUAPL/CIW.